

Construction of 3D Digital Model of a Rock Sample Based on FIB-SEM Data

Iryna Reimers^{*†}, Ilia Safonov^{*}, Ivan Yakimchuk^{*}

^{*}Schlumberger Moscow Research Center,

[†]Moscow Institute of Physics and Technology

Moscow, Russia

irene.ab18@gmail.com, {isafonov, iyakimchuk}@slb.com

Abstract—Focused ion beam tomography (FIB-SEM) is one of the promising methods for studying materials microstructure. The result of the procedure is an image stack of sequential layers of a sample. The reconstruction of the 3D porous structure from FIB-SEM data is an important problem in oil and gas industry for the moment. This paper concerns alignment and segmentation of images with pore-back effect. We introduce a metrics for evaluation of alignment quality and present a new segmentation method based on a marker-controlled watershed. Matrix markers are found with the use of variance filter, and markers of pores — by thresholding and morphological half-gradient. Besides that, a new approach is employed for generation of more reliable synthetic ground truth data. Finally, we evaluate the proposed segmentation method numerically using the synthetic image and manually labelled real data. Our segmentation technique outperforms two existing algorithms.

I. INTRODUCTION

Studying porous materials is of great importance for the oil and gas industry. Precise data about inner structure of oil-bearing rocks enable a construction of digital rock — a digital model of a sample [1, 2], which is used for mathematical simulations of liquid flows in porous media. The goal is to estimate porosity, permeability and strength characteristics of a reservoir. Generally, digital rock is constructed relying on images obtained by X-ray microtomography. However, we need images with higher resolution to study a material at a scale of nanometers. Such images can be obtained by FIB-SEM tomography which resolves details with the size about 5-10 nanometers. This technology is widely used for investigation of rocks, fuel cells electrodes, semi-conductors, nanomaterials, alloys, biological tissues, etc.

The FIB-SEM device uses the combination of focused ion beam (FIB) and scanning electron microscope (SEM). (Fig. 1). The angle between their columns is about 52 degrees. The ion beam removes a thin layer of substance from the sample and then the electron microscope scans the surface [3]. Repetition of these procedures allows to obtain a stack of images corresponding to slices of a rock sample. Previously this technology was used mainly for visual analysis of material structure, but now image processing and segmentation have to be conducted to characterize a sample numerically and build its 3D model.

This paper considers general workflow of construction of 3D digital rock model from a stack of FIB-SEM images and concentrates on alignment and segmentation stages. Section II

describes peculiarities of FIB-SEM images and section III decomposes the problem of building of 3D model on specific consecutive subtasks. Our real and synthetic samples are described in section IV. Section V is devoted to alignment of the image stack and introduces a new metrics for evaluation of alignment quality. In section VI we consider some methods of segmentation, develop a new algorithm, propose metrics for segmentation quality assessment and, finally, present our results. Since alignment and segmentation are quite independent procedures and have their own specific methods, we provide each section with the separate review of prior art.

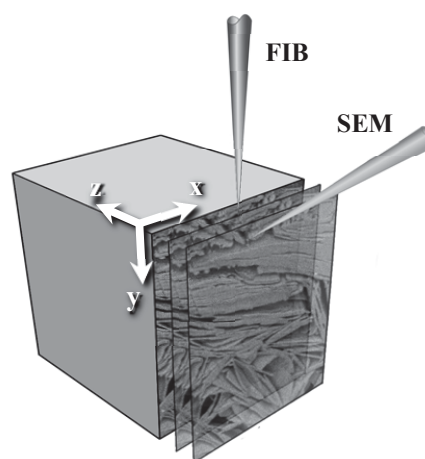


Fig. 1. A scheme of FIB-SEM tomography

II. ANALYSIS OF PECULIARITIES OF FIB-SEM IMAGES

Construction of 3D model from a series of 2D FIB-SEM images is a complicated process due to numerous intensity distortions, artifacts and peculiarities of FIB-SEM images, especially in case of porous media. Some of them are typical for 2D SEM images in general, others are related to FIB-SEM tomography only.

All SEM images are noisy and need to be filtered. Another problem is that the electric charge can be accumulated on the surface despite the conductive covering of the sample. This leads to gradual intensity variations through the image (Fig. 2a) or even bright flares in some places (Fig. 2b). Because of physical reasons sharp edges of pores generate more radiation than smooth ones, so, sometimes a bright halo appears on pore edges (Fig. 2a).

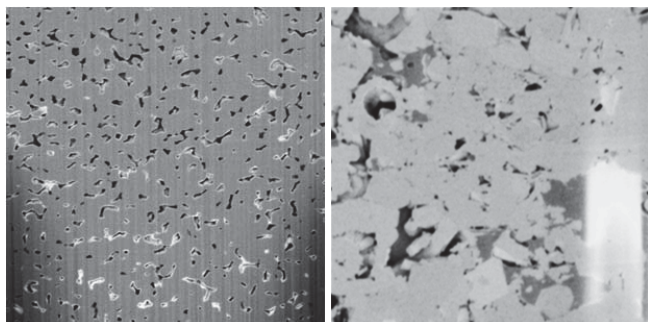


Fig. 2. a) an image with intensity gradient, curtaining and halo [4]; b) an image of a multiphase rock with a flare artifact

Another artifact, so-called curtaining, belongs to FIB-related artifacts. The ion beam can slightly deviate from its initial position while removing a layer, so, we get not flat but ribbed surface and can observe vertical stripes on the image (Fig. 2a, Fig. 3).

The main specific feature of FIB-SEM images in case of porous media is so-called pore-back or shine-through effect. Since pores are transparent, their back side is visible in the current slice, whereas, in fact, it lies in the next layers (examples are shown in Fig. 3). A pore-back side and mineral matrix in the current plane often have similar intensities, and this leads to false segmentation of an image [5]. The situation becomes even more complicated if there are several phases of solid matrix or inclusions (e.g. kerogen) in the rock (Fig. 2b). Multi-class segmentation algorithm should be applied in such case.

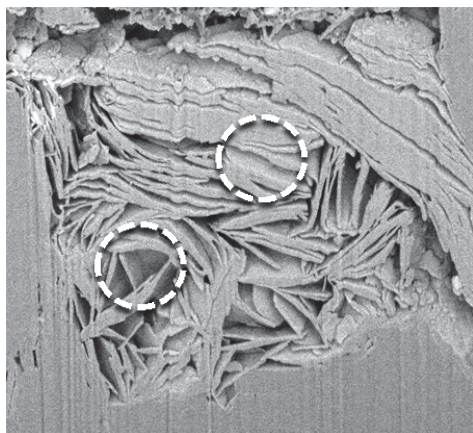


Fig. 3. An example of pore-back effect

One more problem is that images of different slices are displaced relative to each other due to some reasons, such as charge accumulation, mechanical and thermal instabilities during the experiment [6]. Preliminary alignment is made automatically using special reference points that are etched on the sample. Nevertheless, there are still residual displacements between the slices. It can be easily seen in so-called side view when the stack is looked through not in original coordinate plane (xy), but in two other planes (xz) and (yz). Shivering of original frames looks like displacement of rows in side view (Fig. 4). This defect can interfere a lot with segmentation algorithms.

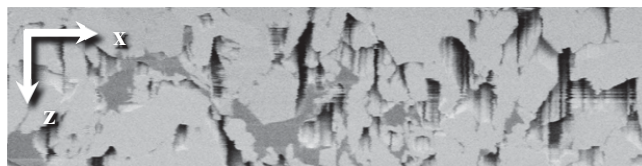


Fig. 4. A side view of a 3D image

Also, during the study of FIB-SEM images, we have observed special cases, when some thin elements (just before being removed by the ion beam) get detached from the matrix and move separately.

III. WORKFLOW FOR BUILDING OF 3D MODEL

Some of considered artifacts occur only in confined places of an image or even can be absent depending on the combination of sample and equipment in each certain case. Other drawbacks (e.g. noise or shivering) cannot be avoided. Despite the fact that complete workflow should cover solutions of all problems listed in section II, in this paper we concentrate on the essential points. Having analyzed FIB-SEM images and papers (e.g. [5], [7-9]), we propose the following workflow for building 3D model of porous media from FIB-SEM images:

- edge-preserving noise suppression;
- precise alignment of images;
- segmentation considering pore-back effect.

Concerning the first stage of the workflow, we need to suppress noise with preserving of edges between pixels that belong to pores and mineral matrix. For this purpose bilateral filter [10], NL-means filter [11] or multi-block bilateral filter [12] can be used. There are two approaches for filtration: processing of each 2D slice or the whole 3D image. For regions with well aligned slices 3D-filtration provides better noise suppression, but in case of significant misalignment it can blur some edges. Therefore, 2D-filtration is preferable. Besides that, separate processing of different slices can be implemented concurrently. Due to parallel processing filtration of the whole 3D image is performed faster.

IV. GROUND TRUTH IMAGES

One of the main obstacles that prevents numerical assessment of algorithms intended for FIB-SEM image processing is a lack of ground truth data. In the paper [13] synthetic test images are generated as a set of spheres and cylinders with predefined sizes. These reference data differ significantly from porous structures used in oil and gas industry for construction of digital rock.

We have taken the following approach to generation of synthetic 3D image of porous media. Segmented 3D X-Ray microtomography image of a real porous sample was used as initial data. The slices of this image are perfectly aligned due to the way they are obtained. Then we rendered this stack as whole 3D structure in Avizo[®] software (Thermo Fisher Scientific, USA) [14]. Standard tools of Avizo allow to cut off (i.e. not to show) required number of slices and in such a way emulate ion milling process. Angle of camera view was set close to the tilt angle of the electron column relative the ion one. Wide capabilities of light settings during visualization

allow to achieve even more similarity. Finally, Gaussian noise was added to the image (Fig. 5).

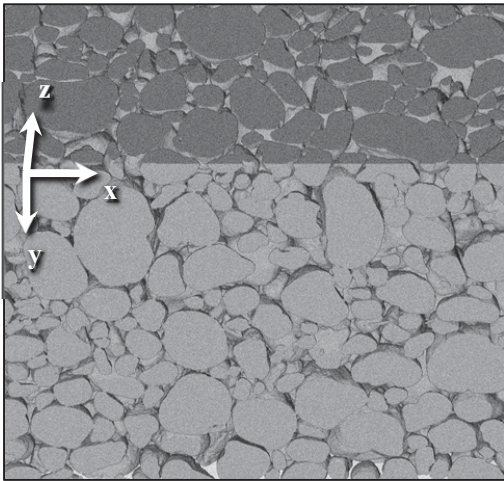


Fig. 5. A synthetic 3D image rendered in Avizo

In addition to the synthetic image we have manually labelled a set of 150 slices of real FIB-SEM image of sandstone. Size of a slice is 200×250 pixels.

V. ALIGNMENT

A. Existing methods

Many authors consider alignment of slices as an important step in preprocessing of a FIB-SEM image. However, in most cases an algorithm or software product is briefly mentioned, and the quality of alignment is not evaluated numerically. All discovered algorithms are based on the comparison of two adjacent slices and on the assumption of their similarity.

The simplest method is to enumerate all possible shifts in some vicinity along x and y axes, and then minimize the difference between images or maximize the correlation coefficient. There are also more complicated algorithms based on image registration. In the paper [5] minimal sum of squared differences is found for intensities less than some threshold in the vicinity ± 10 pixels. Subpixel shifts are calculated using bilinear interpolation.

Nowadays researchers frequently employ various plug-ins for open-source software ImageJ [15-17], [9]. It is mainly one from the following modules for alignment: StackReg [18], JavaSIFT [19] (included in distributive Fiji [20]) and Image Stabilizer [21].

StackReg implements an iterative pyramidal approach for image registration and provides finding of subpixel shifts [22]. At each iteration from low to high resolution, images are approximated with splines. Displacements between them are found by a non-linear method of least squares. JavaSIFT detects feature points in images using Scale-Invariant Feature Transform (SIFT) [23], and then applies RANSAC (RANDOM SAMple Consensus) [24] for finding matrix of transformation from one image to another. Additional limitations such as rigid body model and prohibition of rotation allow to get displacements between images. Image Stabilizer is based on Lucas-Kanade method of calculation of optical flow [25].

Finally, Avizo Software is one of the most common commercial products intended, among other things, for work with FIB-SEM images [14]. This program can also be used for alignment of a stack of images [4]. Alignment of two sequential slices relies on minimization of sum of squared differences.

B. Quality metrics

Displacements of slices become even more obvious in the side view (Fig. 4) of the image. They result in ragged edges between dark pores and light solid matrix, so, we see “comb” structure instead of even edges. The idea of quality metrics is based on evaluation of such structures in 3D image: the fewer “teeth” the “comb” has, the better slices are aligned.

Morphological operations tophat and bothat allow to detect such regions. Tophat is the difference between the original image and its morphological opening. This operation marks small light details in the image. Bothat is the result of subtraction of the original image from its morphological closing; it highlights, on the contrary, small dark regions of the image:

$$\text{tophat}(Im) = Im - \text{opening}(Im) \quad (1)$$

$$\text{bothat}(Im) = \text{closing}(Im) - Im \quad (2)$$

where $\text{opening}(Im)$ is morphological opening, $\text{closing}(Im)$ is morphological closing.

Let us demonstrate the application of tophat and bothat to the binary image and the same image with shifted rows (Fig. 6). Bothat produces only solitary pixels in case of smooth edges (Fig. 7a) and detects shifted rows as indented lines (Fig. 7b). Tophat has the similar effect. Smoothness is considered here rather in visual but not in mathematical sense.

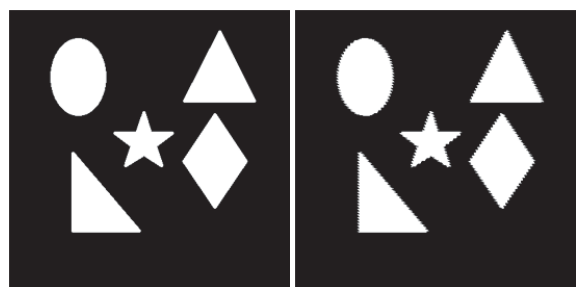


Fig. 6. a) an original binary image b) the same image with shifted rows

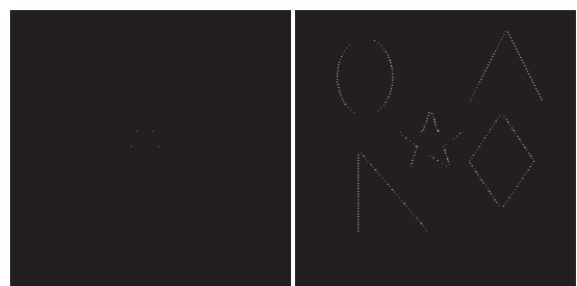


Fig. 7. a) application of tophat to the original image b) application of tophat to the image with shifted rows

This approach is easily generalized for 3D greyscale images. First, 3-dimensional structure element must be used. Since the misalignment results in ragged edges along z-axis (Fig. 4), the structure element must connect the central pixel with pixels along z-axis as well, but not with pixels in (xy) plane. Second, as far as we suppress noise for each slice individually, intensity along z-axis remains inhomogeneous. Thresholding converts the result of tophat and bothat into binary image and makes the criterion insensitive to noise. Let us denote by I' an image which equals to disjunction of thresholded tophat and bothat:

$$I' = (\text{tophat}(Im) > T) \text{ or } (\text{bothat}(Im) > T) \quad (3)$$

where T is predefined threshold. Then we introduce the misalignment metrics as the sum of voxels in I' :

$$C = \text{sum}(I') \quad (4)$$

C. Results

We have aligned the real FIB-SEM image using ImageJ plug-ins JavaSIFT, StackReg, Image Stabilizer and Avizo software, and then applied the described morphological criterion. Fig. 8 shows an example of image I' side view which is calculated from the original and aligned images:



Fig. 8. a) a side view of I' calculated for the original image; b) a side view of I' calculated for the aligned image

Values of misalignment metrics for all methods normalized to the value of the original image are presented in the Table I (less is better).

TABLE I. ALIGNMENT QUALITY FOR VARIOUS SOFTWARE

| Software | C / C_0 |
|------------------------------|-----------|
| JavaSIFT (not subpixel mode) | 0.634 |
| JavaSIFT | 0.204 |
| StackReg | 0.337 |
| Image Stabilizer | 0.198 |
| Avizo | 0.489 |

Based on obtained results we conclude that algorithms with subpixel processing, in a natural way, perform better alignment and decide to use Image Stabilizer.

VI. SEGMENTATION

A. Related works

Many authors note a negative influence of pore-back effect on segmentation of FIB-SEM images, but only in few works specific algorithms are developed [5, 7, 9]. Most of them are based not on simple segmentation of each slice in (xy) plane, but also on analysis of a pixel intensity along z coordinate, that is perpendicular to the milling plane and corresponds to a slice number in 3D image.

Let us consider an exemplary dependence of a pixel intensity on z coordinate (Fig. 9). In the case of a monomineral rock, sharp minima on the graph correspond to the end of mineral matrix and pore beginning (section 1-2). As the number of cut-off slices grows, the pore “opens” and becomes brighter which means the growth of intensity (section 2-3). On the section 3-4 the pore ends, and mineral matrix begins. During the movement through the matrix, the intensity value remains relatively the same until the next minimum comes (section 5-6).

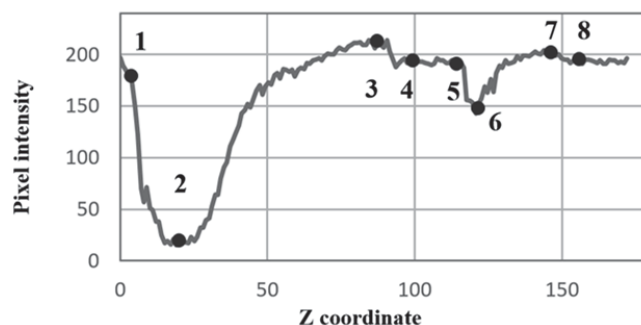


Fig. 9. A dependence of a pixel intensity on z coordinate

In paper [7] authors note instability of algorithms that apply global thresholding for the whole 3D image. They propose analyzing dependences of pixels intensity on z coordinate and finding local minima that correspond to the end of mineral matrix and pore beginning (for example, vicinity of points 2 and 6 in Fig. 9). Current pixel and some previous ones are classified as mineral matrix. Then the result is corrected by means of morphological operations and local thresholding. The segmentation was performed for FIB-SEM images of a synthetic highly-porous silicate material. It differs significantly from porous structure of rocks, and the method cannot be used in our case. In paper [8] the authors analyze several segmentation algorithms, apply them to synthetic data and conclude that the choice of specific algorithm strongly depends on the type of studied sample and its porosity.

In paper [9] marker-controlled watershed transformation [26] is employed for segmentation of porous structures in fuel cells. The authors have developed the following steps for placement of markers in the original image Im :

- Thresholding $F_{GV} = (Im < \text{threshold})$, which highlights low intensity regions, i.e. beginnings of deep pores (for example, vicinity of point 2 in Fig. 9).
- Morphological gradient F_{Grad} [27] gets pixels on edges of regions with different intensities. Using reconstruction by

dilation [28] they also find image F_{\min} that contains the first pixels of local minima with the dynamics (or amplitude) not less than d_{\min} . Intersection $F_{\min(2)} = F_{\min} \cap F_{\text{Grad}}$ corresponds to the first pixels of local minima with dynamics not less than d_{\min} , that are situated on edges of regions with different intensities. Thus, $F_{\min(2)}$ contains initial pore markers.

- Thresholding of morphological positive half-gradient along z coordinate finds homogeneous regions that correspond to mineral matrix (see formula (5)). The result of the operation is marked as F_{Art} .
- Reconstruction by dilation with marker image F_{Art} and mask that equals $\text{NOT}(F_{\min(2)} \cup F_{\text{GV}})$ results in the image F_{Seg} . In other words, F_{Art} “grows” up to beginning of pores, so in the first approximation F_{Seg} represents slightly extended matrix markers, and its negative is a source for pore markers.
- Matrix markers are obtained by erosion of F_{Seg} , and pores markers — by sum of erosions of F_{GV} and negative F_{Seg} .
- Morphological gradient F_{Grad} is used as relief for watershed segmentation.

Trying to apply the described algorithm to rock images we discovered that large pores of high and homogeneous intensity are detected as mineral matrix, which leads to a false segmentation.

One more method for segmentation of FIB-SEM images is described in documentation of Avizo software (Thermo Fisher Scientific, USA) [14]. They also recommend marker-controlled watershed algorithm for slice-by-slice segmentation. Pores markers are placed using threshold transformation and morphological operation both that highlights small dark regions in the image. The algorithm works under the assumption of matrix homogeneity and finds the markers by thresholding of variance filter [29] with kernel size 15-25 pixels. However, large pores can also be quite homogeneous, so it is recommended to define pores after finding matrix pixels in order to “rewrite” false marked pixels. Nevertheless, this does not correct all mistakes because the dark beginning of a pore is not always situated in the slice processed at the moment. Thus, unreliable method for pores detection and slice-by-slice (2D) processing of 3D image are significant drawbacks of the method.

B. Proposed algorithm

We propose an alternative segmentation procedure. Because of the slight changes from pore to matrix in many cases (look at sections 3-4 and 7-8 in Fig. 9) it makes sense to use watershed algorithm to build the missing edge. Our algorithm is three-dimensional, it means that all operations are applied to the whole set of slices. Parts of an image that correspond to mineral matrix are relatively homogeneous in all

directions, so, we threshold 3D variance filter to place mineral matrix markers [29].

Pore markers are found by means of thresholding, because most pores begin from regions with low intensity. Besides that, we use a morphological positive half-gradient:

$$\text{halfgrad}_{\text{plus}}(Im) = \delta(Im) - Im \quad (5)$$

where $\delta(Im)$ is dilation (maximum filter) of the initial image Im . Positive half-gradient marks pixels that are situated near the edges between the regions with different intensities and belong to darker region. Therefore, thresholding of positive half-gradient gives us pore markers (see Fig. 10b).

As a relief for watershed segmentation we use the sum of initial image and its negative half-gradient, where the half-gradient is calculated as:

$$\text{halfgrad}_{\text{minus}}(Im) = Im - \varepsilon(Im) \quad (6)$$

where $\varepsilon(Im)$ is erosion (minimum filter) of Im . This transform highlights pixels near the edge of regions with different intensities that belong to lighter regions, i.e. mineral matrix. Another option of watershed relief is morphological gradient or zero-crossing of Laplacian of Gaussian (LOG).

Fig. 10 demonstrates various steps of algorithm on the side view.

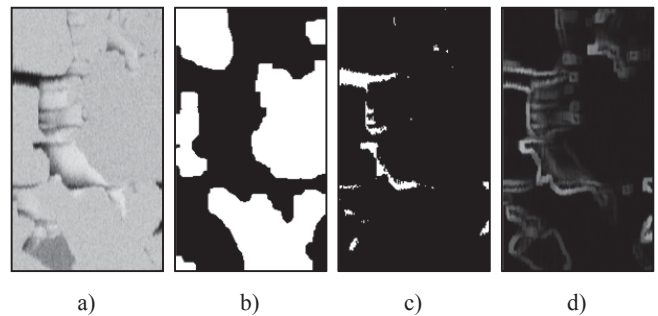


Fig. 10. a) initial image (side view); b) thresholding of the variance filter; c) thresholding of positive morphological half-gradient; d) negative morphological half-gradient.

C. Segmentation criteria

In the paper [30] various criteria of segmentation quality are analyzed. Most of pixel-wise criteria originate from quality metrics for classification. One of the simplest criteria is part of correctly segmented image elements (pixels or voxels):

$$\text{Accuracy} = \frac{tp+tn}{tp+fp+tn+fn} \quad (7)$$

where tp — number of correctly segmented pore elements, tn — number of correctly segmented mineral matrix elements, fp and fn — number of mistakes when matrix elements are classified as pores and vice versa.

Jaccard index is another popular segmentation criterion. Let us denote by G image that sets pore pixels in ground truth (or

reference) image equal to 1, and other pixels equal to zero. D is the same towards segmented image. Then Jaccard index is given by expression:

$$J = \frac{S(G \cap D)}{S(G \cup D)} \quad (8)$$

where $S(x)$ — function that calculates number of non-zero elements in set x .

We should note that pixel-wise segmentation metrics works well only if we have ideal ground truth. In the case of FIB-SEM images there are uncertainties even in manual labelling, so segmentation made by different experts are not the same. Thus, even a quite good algorithm which makes minor mistakes on regions edges is “fined” by a pixel-wise quality criterion. Moreover, small but important regions (for example, in case of low-porosity rock) do not contribute significantly in the final score. Therefore, region-wise criteria are preferable. Ideally, a criterion should give a high score to an algorithm that produce similar shaped pores, but not just pores with the right area.

Antonacopoulos et al. [31] describe a multi-class segmentation measure that was used in document segmentation competition in the scope of International Conference on Document Analysis and Recognition (ICDAR) in 2007. This measure employs the main concept proposed by Phillips and Chhabra [32] for estimation of recognition quality of several primitives of vector graphics such as lines, circles, and arcs. We suppose, this region-based criterion is suitable for considered document segmentation task, but for our problem some points should be changed.

As mentioned before, G and D are images that set pore pixels in ground truth and segmented images equal to 1, other pixels equal to 0. N is the number of connected regions in G , g_k designates k^{th} connected region, $k = 1 \dots N$. In the same way image D sets pore pixels in segmented image equal to one, other pixels equal to zero. There are M connected regions in image D , t^{th} connected region is denoted by d_t , $t = 1 \dots M$.

Let us denote by Gd_t a set of those connected regions in G that have non-empty intersection with region d_t : $Gd_t = \{g | g \in G, g \cap d_t \neq \emptyset\}$. In the same way, Dg_k is a set of connected regions in D that have non-empty intersection with g_k : $Dg_k = \{d | d \in D, d \cap g_k \neq \emptyset\}$.

For each region d_t Intersection over Union $DIOU_t$ is given as:

$$DIOU_t = \frac{S(G \cap d_t)}{S(Gd_t \cup d_t)} \quad (9)$$

where $S(x)$ — function that calculates number of non-zero elements in set x .

For each region g_k Intersection over Union $GIOU_k$ is calculated as:

$$GIOU_k = \frac{S(D \cap g_k)}{S(Dg_k \cup g_k)} \quad (10)$$

We distinguish three cases of correspondence of regions in segmented and reference images to each other (see Fig. 11):

- “one to one” — one segmented region d_t corresponds to one region of reference. This means, image $G \cap d_t$ contains only one connected region and $DIOU_t$ is bigger than some predefined threshold: $DIOU_t > thresh$ (Fig. 11a);
- “one to many” — one segmented region d_t corresponds to several regions from ground truth image, so, the image $G \cap d_t$ contains more than one connected region and $DIOU_t > thresh$ (Fig. 11b);
- “many to one” — several segmented regions corresponds to one region of reference, that means $D \cap g_k$ contains more than one connected region and $GIOU_k > thresh$ (Fig. 11c).

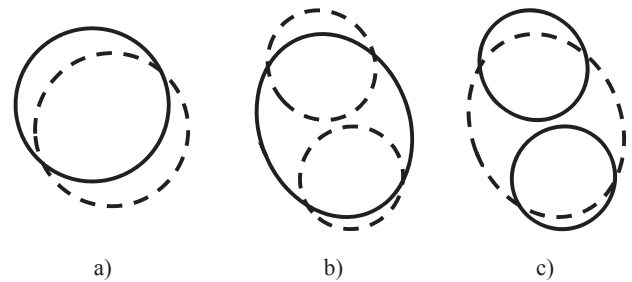


Fig. 11. An illustration of different cases of correspondence of segmented (solid line) and ground truth regions (dashed line).

Then, we calculate numbers of enumerated cases “one to one” n_{oo} , “one to many” n_{om} and “many to one” n_{mo} . Detection rate DR and recognition accuracy RA are defined as:

$$DR = \frac{w_1 n_{oo} + w_2 n_{om} + w_3 n_{mo}}{N} \quad (11)$$

$$RA = \frac{w_4 n_{oo} + w_5 n_{om} + w_6 n_{mo}}{N} \quad (12)$$

where w_i are weights which allow to adjust relative importance of cases. In ICDAR 2007 competition the following weights were used: $w_1 = w_4 = 1, w_2 = w_3 = w_5 = w_6 = 0.75$ [31]. Such parameters give maximum score to one-to-one matches and we use the same weights.

Final segmentation metrics RM is a harmonic mean of DR and RA :

$$RM = \frac{2DR \times RA}{DR + RA} \quad (13)$$

We calculate segmentation metrics slice-by-slice and then average it. Otherwise there is the only one connected region in the whole sample, because almost all pores are connected to each other.

D. Segmentation results for the synthetic image

Our method as well as algorithms used in Avizo and in the paper [9] were implemented with Python. The following parameters were used for segmentation of the synthetic image (Fig. 5):

- gaussian noise: standard deviation $\sigma = 10$;
- bilateral filter from OpenCV library [34]: $d = 11$, $\sigma_{color} = 20$, $\sigma_{space} = 30$;
- the proposed algorithm: threshold for pore markers $threshold_{pore} = 130$, size of structure element for half-gradients $connectivity_{halfgrad} = 7$, threshold for positive half-gradient $threshold_{halfgrad_plus} = 30$, kernel size for variance filter $window_{variance} = 11$, threshold for variance filter $threshold_{variance} = 5$;
- Avizo algorithm: threshold for pore markers $threshold_{pore} = 130$, size of structure element for bothat $connectivity_{bothat} = 9$, threshold for bothat $threshold_{bothat} = 25$, kernel size for variance filter $window_{variance} = 11$, threshold for variance filter $threshold_{variance} = 5$, standard deviation for LOG $\sigma_{LOG} = 3$;
- morphological segmentation [9]: threshold for pore markers $threshold_{pore} = 130$, threshold for morphological gradient $threshold_{morphgrad} = 20$, minimum dynamics $d_{min} = 20$, threshold for positive half-gradient along z axis $threshold_{halfgrad_plus_z} = 2$, size of structure element for half-gradient $connectivity_{halfgrad} = 15$.

Fig. 12 demonstrates ground truth segmentation and the results of three mentioned algorithms.

As illustrated by Fig. 12b), 2D processing of slices gives a disruptive segmentation which does not fit to ground truth and leads to mistakes in the further use of such digital rock. The result of the second algorithm (Fig. 12c) looks better, but segmentation of the first slices is incorrect. Segmentation quality was calculated for all three algorithms. We used the following segmentation criteria: the part of correctly segmented voxels $Accuracy$, Jaccard index J and averaged by slices

region-wise metrics RM_{avg} . The results are shown in the Table II. Despite a visual evidence that the proposed algorithm works better, its $Accuracy$ value is little lower. This proves once again that pixel-wise metrics are not suitable for our problem. Morphological method [9] has the highest Jaccard index but unreasonably low score from the region-wise metrics. The reason is that it produces over-segmentation and almost all segmented regions are connected with each other, which is fined by the region-wise metrics. None of the criteria is perfect, but segmentation of the proposed algorithm seems better than others (see Fig. 12).

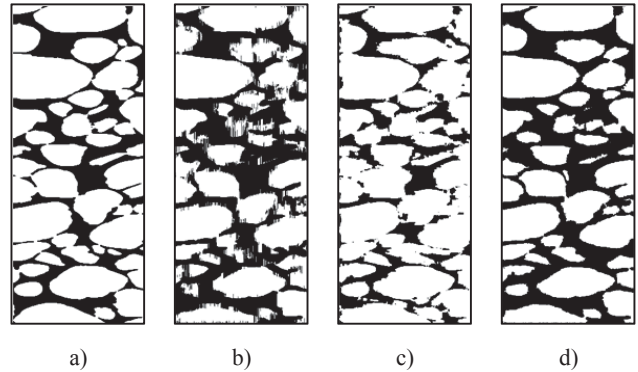


Fig. 12. A) ground truth image (side view); b) result of Avizo algorithm; c) result of morphological segmentation from the paper [9]; d) results of the proposed algorithm.

TABLE II. SEGMENTATION QUALITY OF THE ALGORITHMS (SYNTHETIC IMAGE)

| | Avizo algorithm | Morphological segmentation [9] | Proposed algorithm |
|-------------------------|-----------------|--------------------------------|--------------------|
| <i>Accuracy</i> | 0.82 | 0.87 | 0.84 |
| <i>J</i> | 0.74 | 0.83 | 0.77 |
| <i>RM_{avg}</i> | 0.45 | 0.14 | 0.65 |

E. Segmentation results for the real image

The following parameters were used for segmentation of the real image (Fig. 4):

- bilateral filter from OpenCV library [34]: $d = 11$, $\sigma_{color} = 20$, $\sigma_{space} = 30$;
- proposed algorithm: threshold for pore markers $threshold_{pore} = 110$, size of structure element for half-gradients $connectivity_{halfgrad} = 7$, threshold for positive half-gradient $threshold_{halfgrad_plus} = 60$, kernel size for variance filter $window_{variance} = 15$, threshold for variance filter $threshold_{variance} = 4$;
- Avizo algorithm: threshold for pore markers $threshold_{pore} = 110$, size of structure element for bothat $connectivity_{bothat} = 9$, threshold for bothat $threshold_{bothat} = 25$, kernel size for variance filter

$window_{variance} = 15$, threshold for variance filter
 $threshold_{variance} = 4$, standard deviation for LOG
 $\sigma_{LOG} = 3$;

- morphological segmentation [9]: threshold for pore markers $threshold_{pore} = 110$, threshold for morphological gradient $threshold_{morphgrad} = 20$, minimum dynamics $d_{min} = 30$, threshold for positive half-gradient along z axis $threshold_{halfgrad_plus_z} = 2$, size of structure element for half-gradient $connectivity_{halfgrad} = 15$.

Fig. 13 demonstrates segmentation that is correct according to expert's opinion and the results of three mentioned algorithms.

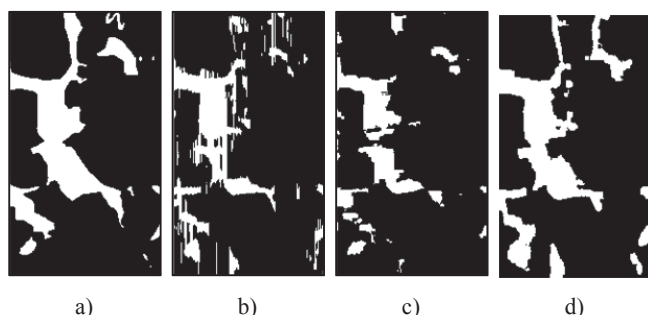


Fig. 13. a) ground truth image (side view); b) result of Avizo algorithm; c) result of morphological segmentation from paper [9]; d) results of proposed algorithm.

Segmentation quality metrics are shown in the Table III. As concluded from the results for synthetic image, pixel-wise metrics is inconsistent and cannot be used in our problem. Two other indices gave the maximal score to the proposed algorithm.

TABLE III. SEGMENTATION QUALITY OF THE ALGORITHMS (REAL IMAGE)

| | Avizo algorithm | Morphological segmentation [9] | Proposed algorithm |
|-------------------------|-----------------|--------------------------------|--------------------|
| <i>Accuracy</i> | 0.87 | 0.90 | 0.89 |
| <i>J</i> | 0.47 | 0.53 | 0.57 |
| <i>RM_{avg}</i> | 0.09 | 0.22 | 0.25 |

VII. CONCLUSION

We have considered the main difficulties that arise during construction of 3D digital model of a rock sample based on FIB-SEM data. Then, the most common software for alignment of an image stack is compared using quality metrics based on morphological operations. According to the results, ImageJ plug-ins Image Stabilizer performed the best alignment.

We have also developed the algorithm for segmentation of 3D FIB-SEM images of rocks that is the most important step in construction a digital model of the sample. The results of the method were evaluated with several criteria of segmentation quality using synthetic data and manually labeled images of a real sample. We should also note that, first, a new method was

proposed for generation of more reliable synthetic data. Second, the authors have not encountered publications, where the results would be estimated not on synthetic FIB-SEM images but on natural samples of rock. According to the results, our algorithm segments rocks with moderate porosity better than existing methods. Nevertheless, the obtained values of segmentation quality are still far away from perfect. One of the reasons is uncertainty of ground truth data since some edges have so slight gradient that it complicates correct manual segmentation. On the other hand, improvement of segmentation algorithm is also needed, especially in case of high noise level and several mineral types in the sample.

REFERENCES

- [1] D. Koroteev, O. Dinariev, N. Evseev, D. Klemin, A. Nadeev, S. Safonov, O. Gupinar, S. Berg, C. van Kruijsdijk, R. Armstrong, M.T. Myers, L. Hathon and H. de Jong, "Direct hydrodynamic simulation of multiphase flow in porous rock", *Petrophysics*, vol.55, № 04, 2014, pp. 294-303.
- [2] C.F. Berg, O. Lopez and H. Berland, "Industrial applications of digital rock technology", *Journal of Petroleum Science and Engineering*, vol. 157, 2017, pp. 131-147.
- [3] L. Holzer and M. Cantoni, "Review of FIB Tomography", *Nanofabrication Using Focused Ion and Electron Beams: Principles and Applications*. New York: Oxford University Press, 2012, pp. 410-435.
- [4] N.J. Welch, F. Gray, A.R. Butcher, E.S. Boek and J.P. Crawshaw, "High-Resolution 3D FIB-SEM Image Analysis and Validation of Numerical Simulations of Nanometre-Scale Porous Ceramic with Comparisons to Experimental Results", *Transport in Porous Media*, vol. 118, № 3, 2017, pp. 373-392.
- [5] M. Salzer, S. Thiele, R. Zengerle and V. Schmidt. On the importance of FIB-SEM specific segmentation algorithms for porous media, *Materials Characterization*, vol. 95, 2014, pp. 36-43.
- [6] K. Lepinay and F. Lorut, "Three-dimensional semiconductor device investigation using focused ion beam and scanning electron microscopy imaging (FIB/SEM Tomography)", *Microscopy and Microanalysis*, vol. 19, № 1, 2013, pp. 85-92;
- [7] M. Salzer, A. Spettl, O. Stenzel, J.H. Smätt, M. Lindén, I. Manke and V. Schmidt, "A two-stage approach to the segmentation of FIB-SEM images of highly porous materials", *Materials Characterization*, vol. 69, 2012, pp. 115-126.
- [8] M. Salzer, T. Prill, A. Spett, D. Jeulin, K. Schladitz and V. Schmidt, "Quantitative comparison of segmentation algorithms for FIB-SEM images of porous media", *Journal of microscopy*, vol. 257, № 1, 2015, pp. 23-30.
- [9] T. Prill, K. Schladitz, D. Jeulin, M. Faessel and C. Wieser, "Morphological segmentation of FIB-SEM data of highly porous media", *Journal of microscopy*, vol. 250, № 2, 2013, pp. 77-87.
- [10] C. Tomasi and R. Manduchi, "Bilateral filtering for gray and color images", *Sixth International IEEE Conference on Computer Vision*, 1998, pp. 839-846.
- [11] A. Buades, B. Coll and J.M. Morel, "A non-local algorithm for image denoising", *IEEE Computer Society Conference on Computer Vision and Pattern Recognition*, vol. 2, 2005, pp. 60-65.
- [12] I.V. Safonov, I.V. Kurilin, M.N. Rychagov and E.V. Tolstaya, *Adaptive Image Processing Algorithms for Printing*. Singapore: Springer, 2018.
- [13] T. Prill and K. Schladitz, "Simulation of FIB-SEM Images for Analysis of Porous Microstructures", *Scanning*, vol. 35, № 3, 2013, pp. 189-195.
- [14] Avizo official website, Web: <https://www.thermofisher.com/ru/ru/home/industrial/electron-microscopy/electron-microscopy-instruments-workflow-solutions/3d-visualization-analysis-software.html>.
- [15] ImageJ official website, Web: <http://imagej.net>
- [16] T.A. Dewers, J. Heath, R. Ewy and L. Duranti, "Three-dimensional pore networks and transport properties of a shale gas formation determined from focused ion beam serial imaging", *International Journal of Oil, Gas and Coal Technology*, vol. 5, № 2-3, 2012, pp. 229-248.

- [17] S. Gaboreau, J.C. Robinet, D. Prêt, "Optimization of pore-network characterization of a compacted clay material by TEM and FIB/SEM imaging", *Microporous Mesoporous Mater.*, vol. 224, 2016, pp. 116-128.
- [18] P. Thévenaz, ImageJ plugin for the recursive alignment of a stack of images, Web: <http://bigwww.epfl.ch/thevenaz/stackreg/>
- [19] S. Saalfeld, ImageJ plugin for the linear stack alignment with SIFT, Web: https://imagej.net/Linear_Stack_Alignment_with_SIFT
- [20] J. Schindelin, I. Arganda-Carreras, E. Frise, V. Kaynig, M. Longair, T. Pietzsch, S. Preibisch, C. Rueden, S. Saalfeld, B. Schmid, J.-Y. Tinevez, D.J. White, V. Hartenstein, K. Eliceiri, P. Tomancak and A. Cardona, "Fiji: an open-source platform for biological-image analysis", *Nature methods*, vol. 9, № 7, 2012, pp. 676-682.
- [21] K. Li, ImageJ alignment plugin Image Stabilizer, Web: http://www.cs.cmu.edu/~kangli/code/Image_Stabilizer.html
- [22] P. Thevenaz, U.E. Ruttimann, M. Unser, "A pyramid approach to subpixel registration based on intensity", *IEEE transactions on image processing*, vol. 7, № 1, 1998, pp. 27-41.
- [23] D.G. Lowe, "Distinctive image features from scale-invariant keypoints", *International journal of computer vision*, vol. 60, № 2, 2004, pp. 91-110.
- [24] M.A. Fischler, R.C. Bolles, "Random sample consensus: a paradigm for model fitting with applications to image analysis and automated cartography", *Communications of the ACM*, vol. 24, № 6, 1981, pp. 381-395.
- [25] B. D. Lucas and T. Kanade, "An iterative image registration technique with an application to stereo vision", in *Proc. DARPA Image Understanding Workshop*, Apr. 1981, pp.121-130.
- [26] S. Beucher and F. Meyer, "The morphological approach to segmentation: the watershed transformation", *Optical Engineering*. New York-Marcel Dekker Incorporated, vol. 34, 1992, pp. 433-433.
- [27] P. Soille, *Morphological image analysis: principles and applications*. New York: Springer Science & Business Media, 2013.
- [28] L. Vincent, "Morphological grayscale reconstruction in image analysis: applications and efficient algorithms", *IEEE transactions on image processing*, vol. 2, № 2, 1993, pp. 176-201.
- [29] A. Fabijańska, "Variance filter for edge detection and edge-based image segmentation, in *Proc. VIIIth International IEEE Conference on Perspective Technologies and Methods in MEMS Design (MEMSTECH)*, 2011, pp. 151-154.
- [30] J. Pont-Tuset, F. Marqués, "Supervised evaluation of image segmentation and object proposal techniques", *IEEE transactions on pattern analysis and machine intelligence*, vol. 38, № 7, 2016, pp. 1465-1478.
- [31] A. Antonacopoulos, B. Gatos, D. Bridson, "ICDAR2007 Page Segmentation Competition", in *Proc. IEEE International Conference on Document Analysis and Recognition (ICDAR 2007)*, 2007, pp. 1279-1283.
- [32] I.T. Phillips, A.K. Chhabra, "Empirical performance evaluation of graphics recognition systems", *IEEE Transactions on Pattern Analysis and Machine Intelligence*, vol. 21, № 9, 1999, pp. 849-870.
- [33] J. Pont-Tuset, F. Marqués, "Measures and meta-measures for the supervised evaluation of image segmentation", in *Proc. IEEE Conference on Computer Vision and Pattern Recognition*, 2013, pp. 2131-2138.
- [34] Official website of computer vision library OpenCV, Web: <http://opencv.org> (19.11.2018).